M. Cinelli, S. Puccetti, M. Lavagna, P. Lunghi, G. Pucacco
High Energy Modular Ensemble of Satellites Mission: Towards the Final Full Constellation
Acta Astronautica, Vol. 189, 2021, p. 129-142
doi:10.1016/j.actaastro.2021.08.024

High Energy Modular Ensemble of Satellites mission: towards the final Full Constellation

Marco Cinelli[a,*], Simonetta Puccetti[b], Michèle Lavagna[c], Paolo Lunghi[c], Giuseppe Pucacco[d]

[a] *Department of Mathematics, University of Roma Tor Vergata, Via della Ricerca Scientifica 1, 00133 Roma, Italy*
[b] *Agenzia Spaziale Italiana-Unità di Ricerca Scientifica, Via del Politecnico, 00133 Roma, Italy*
[c] *Department of Aerospace Science and Technology (Dipartimento di Scienze e Tecnologie Aerospaziali), Politecnico di Milano, Via La Masa 34, 20156 Milano, Italy*
[d] *Department of Physics, University of Roma Tor Vergata, Via della Ricerca Scientifica 1, 00133 Roma, Italy*

Abstract

The *High Energy Modular Ensemble of Satellites* (HERMES) project intends to build an all-sky monitor operating from keV to MeV for the detection and localisation of transient events, like gamma ray bursts. HERMES is a modular observatory composed by detectors on-board of nanosatellites. HERMES aims to revolutionise the world of multi-messenger astrophysics thanks to the innovative concept of a modular instrument based on small satellites and characterised by reduced design and development times and low costs, in the face of high technological content and scientific profile of the mission.

A first part of the project, HERMES Technological Pathfinder, composed of three CubeSats, aims to demonstrate the feasibility of detecting transient phenomena in high energy with small satellites. The next phase of the project, HERMES Scientific Pathfinder, will expand the constellation up to six satellites, allowing routinely accurate triangulation measurements.

This paper presents an analysis that aims to be propaedeutic for the design of the final HERMES Full Constellation, which will be an all-sky monitor made

*Corresponding author
Email addresses: marco.cinelli@uniroma2.it (Marco Cinelli), simonetta.puccetti@asi.it (Simonetta Puccetti), michelle.lavagna@polimi.it (Michèle Lavagna), paolo.lunghi@polimi.it (Paolo Lunghi), pucacco@roma2.infn.it (Giuseppe Pucacco)

up of tens/hundreds of nanosatellites in Low Earth Orbit with a total effective area of $\sim m^2$. An adequate number of nanosatellites, simultaneously detecting a transient, provides a source localisation accuracy of the order of magnitude of few arcmin and large effective area. The objective of this work is to define possible strategies of injection in orbit of the complete constellation. In this first analysis we used only the number of triangulable Gamma Ray Bursts (simultaneously detected by at least three nanosatellites) as discriminating factor in order to maximise the constellation performance. By achieving the goal of at least a mean number of 20 Gamma Ray Bursts triangulated per nanosatellite over the two years life-time, optimal configurations for the complete constellation, consisting of seven to fourteen CubeSats, have been identified.
Keywords: Satellite constellation, Gamma-ray Burst, CubeSat Mission, HERMES project, Multi-messenger astrophysics, Transient events

1. Introduction

The fast detection and positioning of Gamma Ray Bursts (GRBs) is one of the challenges of the contemporary science, with many implications in different fields of astrophysics [1, 2, 3]. Several space missions have shown the great utility of space platforms in detecting high-energy photons [4, 5, 6, 7, 8, 9, 10, 11]. These missions are characterised by long development time and very high costs [12, 13].

In this context, the *High Energy Modular Ensemble of Satellites* (HERMES) aims to realise a new generation instrument for the observations of high-energy transients characterised by a different approach from that commonly adopted for space-based observatories. The HERMES concept is an experiment distributed over several units, up to tens/hundreds simple units. The main advantages of the HERMES strategy with respect to traditional High-Energy Astrophysics experiment are: modularity and quick development with limited costs [14, 15, 16, 17]. The mission space segment consists of 3-U CubeSat ($30\,\mathrm{cm} \times 10\,\mathrm{cm} \times 10\,\mathrm{cm}$) [18, 19, 20], in Low Earth Orbit (LEO), with a collect-

ing area ~ 50 cm^2, operating in $\sim 3 - 300$ keV energy range [21]. Therefore the total payload is distributed over several tens/hundreds of such units, and a total sensitive area of the order of magnitude of $\sim$m^2 can be reached. HERMES aims to play a key role in multi-messenger astrophysics in the coming decades [14, 22] through the prompt and accurate localisation of bright X-ray/soft γ-ray transients such as GRBs and will allow to investigate the temporal structure of GRBs down to fractions of micro-seconds.

The first part of the project, HERMES Technological Pathfinder (HTP), actually ongoing, is composed of three CubeSats 3U financed by the Italian space agency (ASI, Agenzia Spaziale Italiana) and by the Italian national Ministry of Education, University and Research (MIUR, Ministero dell'Istruzione, dell'Università e della Ricerca). This part of the project aims to demonstrate the feasibility of detecting high energy photons from astronomical sources with small satellites. The next phase of the project, HERMES Scientific Pathfinder (HSP), composed of a further three 3U CubeSats funded by the European Union through the Horizon 2020 Research and Innovation Program (Grant Agreement No. 821896), will expand the constellation up to six satellites, for a total sensitive area of at least $300\,\mathrm{cm}^2$ [16], improving the accuracy in triangulation measurements. Moreover, the Italian Space Agency approved and funded the participation to the SpIRIT (Space Industry Responsive Intelligent Thermal nanosatellite) CubeSat. The SpIRIT project, which is supported by the Australian Space Agency and led by University of Melbourne, will host an HERMES-like detector thus providing a seventh unit to the HERMES constellation [14, 23]

The mission design and performance of the constellation composed by the nanosatellites of the HTP and HSP missions, in orbit starting from and 2022/beginning 2023, has been deeply analysed in [24, 25]. The HERMES-TP/SP payload (see Fig. 1) was conceived and designed by the University of Cagliari and Istituto Nazionale di Astrofisica (INAF); it is described in detail in [17, 22, 23]. The satellite platform is developed by the Politecnico di Milano which, in collaboration with Istituto Nazionale di Alta Matematica (INdAM) and the University of

Rome Tor Vergata, has been responsible for the HTP mission analysis package [26].

HTP and HSP missions are pathfinders devoted to test the feasibility of the experiment, which has been designed to detect GRBs and localise them by the temporal triangulation method, i.e., by measuring the time delay between the arrival times of the same wave front in at least three different satellites. A further development of the mission is the extension of the constellation to a much greater number of satellites, up to tens/hundreds of CubeSats. This HERMES full constellation (HFC) will allow to increase the total sensitive area up to the order of one square meter, distributed on all the constellation satellites. The HERMES localisation capability is directly proportional to the number of the constellation satellites observing simultaneously the same event and to the average baseline between them [14]. Therefore a source localisation accuracy of the order of magnitude of several arcmin can be reached, for transients with short time scale (<ms) variability [22], using an adequate number of nanosatellites on opportune orbital planes, which simultaneously detect a transient.

This paper presents an analysis that aims to be propaedeutic for the design of the HERMES Full Constellation (HFC) mission. For the present analysis we have considered constellations composed by a number of spacecraft greater than six and taken into account orbital planes with quasi-equatorial and quasi-polar inclinations. A significant difference between the constellation design presented here and HTP, HSP missions is that there are no attitude control manoeuvres aimed at obtaining an optimal pointing strategy (see [25]) to maximise the number of triangulable GRBs. This choice was made in order to reduce the complexity of a constellation design which looks towards HFC. Therefore the purpose of this study is to evaluate the performance obtainable from a constellation that increases the dimensions of those of the HTP and HSP missions. In this analysis we chose to evaluate the performance margins by using only the number of triangulated GRBs (i.e., simultaneously detected by at least three nanosatellites) over the life time of each single satellite, that each additional CubeSat can offer. Using this parameter, we intend to answer two main questions: considering

all the mission constraints, what are the maximum performances obtainable from the constellation as a function of the number of satellites that compose it? Is there a limit size of the constellation beyond which adding satellites causes an unacceptable decline in performance? The paper will try to estimate the maximum performance obtainable from the constellation as a function of the number of satellites composing it, starting from the minimum number of seven units. It is important to remark that the main goal which guided the analysis was the possibility to detect and triangulate the greatest number of GRBs (over the life time of each single satellite), leaving other relevant aspects (e.g., the accuracy of the positioning of the transient events or the effective area) for future analysis. In this way, we want to identify the optimal strategy for placing satellites into orbit in terms of the number of CubeSats that have to fly at the same time.

In Section 2 the mission scenario and the developed software tool are described. Section 3 presents the analysis aimed at identifying nominal orbits, while Section 4 discusses the nominal configurations of the constellation. In Section 5 the robustness analysis regarding the perturbative effects of atmospheric drag and solar radiation pressure, and the consequences of early failures are evaluated.

2. Mission scenario

As mentioned, the considered space segment is composed of at least 7 spacecraft (S/C) in Low Earth Orbit. In this work the possibility of modulating the constellation will be provided in order to maintain performance, described in terms of mean GRBs for S/C observable over the lifetime (2 yrs), approximately constant. The definition of the mission scenario (scientific objectives and requirements, and software tool), leads to the identification of the nominal orbits and configurations.

2.1. HERMES Full Constellation scientific objectives

The HFC mission aims to reach high-level scientific objectives, the main of which is to achieve all-sky coverage with a flux sensitivity of $\sim 0.2\,\mathrm{ph/cm^2/s}$ for

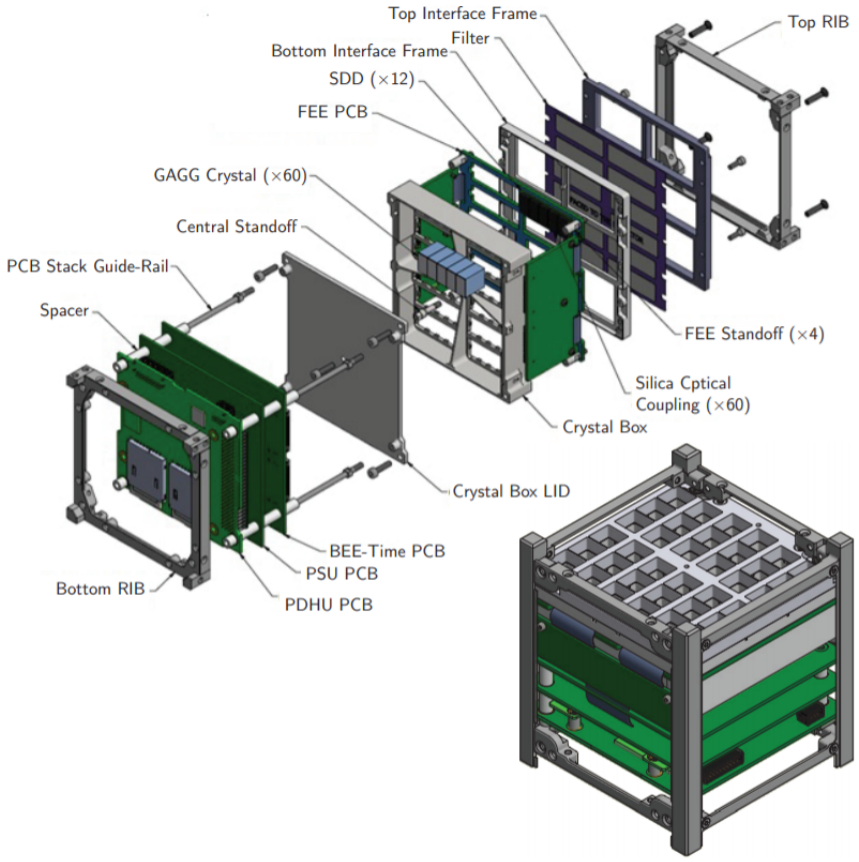

Figure 1: Structure of the HERMES X-/γ-ray detector (figure taken from [17]).

short GRBs in the energy range 50-300 keV [14]. Regarding the localisation, HFC aims to accuracy of bright long GRBs better than $15'$ on each coordinate, corresponding to an error box of $<0.2\,\mathrm{deg}^2$. Such accuracy would allow prompt identification of the transient counterpart at different wavelengths, greatly easing the multi-wavelength follow-up. In case of short GRB, a localisation better than 1 deg in both coordinates, corresponding to an error box of $\sim 3\,\mathrm{deg}^2$, would allow prompt identification of the electromagnetic counterpart of a GWE (Gravitational Wave Event) and guide prompt multi-wavelength follow-up facilitating the identification of the event's host-galaxy in a volume a factor of $\sim$10 larger than the case of the GW170817 (see [14] for more details). The accuracy in determining the position (σ_{PA}, position accuracy) can be approximated by the following simple formula:

$$\sigma_{PA} \sim \frac{\sqrt{\sigma_{delay}^2 + \sigma_{TPOS}^2 + \sigma_{TIME}^2 + \sigma_{sys}^2}}{\overline{AB}\sqrt{N-3}} \quad \text{with} \quad N > 3 \tag{1}$$

where σ_{delay} is the error on the delay (e.g., obtained applying cross-correlation techniques between two light curves), σ_{TIME} is the uncertainty on absolute time of the collected photons, σ_{TPOS} is the error due to the uncertainty on the position of the satellite, σ_{sys} is a systematic uncertainty, $\overline{AB}$ is the Average Baseline, namely the average distance between detectors, and N is the number of detectors observing a given event simultaneously. A detailed description of the terms that appear in Eq. (1) is proposed in [14], but the aspect that is most relevant for the present analysis is that σ_{PA} is a function that varies according to $1/\sqrt{N-3}$. This implies that triangulation accuracy should improve if a very large number of satellites observes the same event. This is true except for σ_{sys}, especially for the faintest GRB population, and which will be better investigated with HERMES pathfinder data. In other words, by increasing N, the sensitivity improves as long as the other terms in Eq. (1) are kept under control. Nevertheless, the analysis of the data of the HTP and HSP missions should allow a better knowledge of the systematic errors. On the other hand,

when many satellites observe the same event, the ratio between the total number of triangulated GRBs and the S/C number dramatically decreases. Moreover, to achieve an all sky coverage monitor, it is necessary at least one of the following two alternatives: a) to consider orbits with non-equatorial inclination; b) resort to attitude manoeuvres for scientific pointing [27]. In the described scenario, the present work proposes to be a preliminary analysis aimed at identifying the limits of constellations in which redundancies are reduced (and therefore the parameter GRBs per spacecraft is maximised). The proposed solutions can be replicated in a modular way, up to a constellation composed of tens/hundreds of nanosatellites, so that a given event is observed simultaneously by a large number of detectors. Furthermore, it can drive the choice concerning the execution of attitude control manoeuvres. A constellation consisting of such a number of units would allow a total collecting area of the order of a few m^2 and feeding light curves of relatively bright GRBs ($>10\,ph/s/cm^2$) with a few counts every 10 μs, thus allowing to fully exploit the good time accuracy of the mission (better than a few hundred nanoseconds).

2.2. Mission Analysis requirements

The mission requirements and constraints have been agreed between the different parts of the project in order to maximise the scientific return of the mission. The main Mission Analysis requirements taken into account are listed below. With a few exceptions, they are the same as those of the HERMES technological pathfinder mission.

- *Orbital requirements.* Since the radiation environment strongly depends on orbit altitude and inclination, the altitude of the operational orbit shall be lower than 600 km to preserve the payload. In fact orbits with altitude higher than 600 km would imply a lifetime of a few months. On the other hand, since there are no station-keeping manoeuvres, it is necessary to consider only altitudes greater than 500 km to avoid that the perturbative effects of atmospheric drag cause the de-orbiting of the CubeSats before the end of the operational life of each small satellite (2 yrs). Indeed, as

demonstrated in [28], the trapped particle fluxes dramatically increase for inclinations greater than 30 degrees, therefore the duty cycle is drastically reduced above this value. Moreover, in [28] it is also shown how, within the orbits with a high inclination (>60°), the quasi-polar orbits have a higher duty cycle. Therefore, considering the FOV of the instrument (see the *Field of View* item below), for the observation of astronomical events up to mid-latitudes, equatorial inclinations are preferable. On the other hand, for observing astronomical sources at high latitudes, quasi-polar orbits are preferable (and, above all, sun-synchronous orbits for launch opportunities). The minimum mission duration shall be 2 yrs.

- *Attitude manoeuvres.* Only a zenithal pointing (maintained by the HERMES's spacecraft attitude control subsystem) can be considered in order to fulfil the requirement according to which each spacecraft shall not perform attitude manoeuvres aiming to obtain optimal pointing which, in general, does not coincide with the zenithal one. This requirement is one of the main differences with respect to the HTP/HSP, and it has been introduced with the purpose to simplify the operation phase of a potentially very large constellation, for which the optimal pointing strategy adopted for the Pathfinder missions [25] cannot be feasible.

- *Forbidden regions.* The detectors on board each satellite shall not be operative while the spacecraft is passing inside forbidden regions, which are the 'High flux regions' corresponding to the South Atlantic Anomaly (SAA) and the high radiation flux polar regions. In Section 3, the forbidden regions are shown and a dedicated analysis allows the identification of the inclinations that minimise the passages of the spacecraft over them.

- *Field of View.* The effective Field of View (FoV) for each satellite is defined as the portion of the celestial sphere with and angular distance of 60° with respect to the detector pointing direction (Full Width at Half Maximum of the instrument sensitivity). For the FoV an average inclination of 45°

respect to the x and y axes of the Local Vertical, Local Horizontal (LVLH) reference frame, centered on the spacecraft, has been considered.

- *FoV overlapping.* A group of co-observing S/C (N_{co-obs}) is composed by at least three active payloads having FoVs overlapping. The co-observing group is active and able to perform triangulation measurements to localise transient events such as GRB and the satellite FoVs overlappings are computed. A satellite is considered active whenever it respects the radiation flux requirements, i.e., when it is outside of all the forbidden regions.

- *Physical baseline.* The physical baseline shall be ≥ 1000 km between any pair of elements in a group of N_{co-obs} satellites.

- *Projected baseline.* Taking into account that the mean pointing direction of a group of co-observing satellites shall be computed as the arithmetic mean of the N_{co-obs} line of sight (LoS) directions (the arithmetic mean of the N_{co-obs} LoS versors), it is possible to compute the so-called 'projected baseline' between any pair of the N_{co-obs} elements over the mean pointing direction. It is required that the projected baseline shall be ≥ 1000 km for at least two pairs of elements in a group of N_{co-obs} satellites. This requirement is necessary because the actual uncertainty of the position reconstruction is inversely proportional to the mean time delay with which the same GRB is detected among different sensors. This delay in time is proportional to the average distance between co-observing satellites, projected along the mean pointing direction. Therefore baselines much larger than the requirement would be desirable either for a better localisation either to evaluate all statistic and systematic effects. On the other hand, as shown below, without pointing manoeuvres, the overlap between different FoVs decreases with increasing projected baselines grow.

At any epoch, each point in the sky visible by at least one active triplet is considered as observable; the total area observed at any time is computed by integrating the observable points over the whole celestial sphere. The to-

tal observable area is measured in sr. The instantaneous observable area is integrated over the whole mission lifetime (Time Area parameter, tA). The total number of the triangulated GRBs is computed using the conversion factor $\alpha_{GBM} = 0.083\,\mathrm{GRB/sr/day}$ deduced from the scientific return obtained by the Fermi Observatory [9, 29]. This conversion factor is realistic for the HERMES mission since, as reported in [14], considering the mock population produced and developed in [30], the majority of the Fermi/GBM GRBs should be detected also by HERMES pathfinder. HERMES payload misses some of the faintest/hardest GRBs, but gain some soft GRBs (thanks to the broad band extending to soft energies, inaccessible to the Fermi/GBM). For the full constellation, the triangulation of $\sim$20 GRB/spacecraft during the 2-years lifetime has been set as a goal. For this purpose, we introduce a performance efficiency parameter denoted with the η symbol; it must be interpreted as follows: the total number of GRBs detected by at least three units (so triangulable) during the lifetime (2 years) is divided by the number of satellites composing the constellation, therefore it is expressed in GRB/spacecraft/2y. Even if the actual number of GRBs detected by each unit will be greater than 20, the adoption of this efficiency parameter allows to compare the performance, in terms of scientific return per spacecraft, achieved by constellations of different size. The goal of 20 GRB/spacecraft has been identified by the HTP and HSP mission analysis: Monte Carlo simulations have shown how, for a constellation of 6 equatorial satellites (3 HTP + 3 HSP nanosatellites) with zenithal pointing, an upper limit of $\sim$ 120 GRBs in 2 years can be triangulated [25, 27]. This constraint is mandatory for equatorial satellites, where it is demonstrated that it can be achieved; whilst, for satellites in quasi-polar orbit, the goal is to reach the highest value of triangulated GRBs taking into account all the other constraints. The η parameter is closely related to economic and practical feasibility. On the one hand, the construction and orbit injection of each satellite has an economic cost; but, on the other hand, this parameter remains consistent with the requirements only if the units of each constellation are able to operate simultaneously. Therefore it is necessary to provide for the launch of additional satellites to ensure the continuous turnover

of the constellation, allowing the nominal units to operate simultaneously.

2.3. Mission analysis software

The scientific performance of the constellations has been evaluated using dedicated software tools developed specifically for these analyses. The developed software-package includes two main blocks: the orbital propagators and the visibility tool. Three different propagation profiles have been provided for orbital propagators:

- *Low Precision Orbital Propagator* (LPOP): is a fast propagator that takes into account only the effects of polar oblateness (J_2 zonal harmonic). This profile was used only for the analysis of the optimal inclination which does not require particular accuracy in propagation.

- *High Precision Orbital Propagator 1* (HPOP1): is an high-fidelity propagator which takes into account the Earth geopotential based on EGM2008 gravity model [31] up to 30th order and degree and the lunisolar third-body perturbations. The Sun and the Moon positions are estimated with the DE431 Ephemeris model [32];

- *High Precision Orbital Propagator 2* (HPOP2): a high fidelity propagator which includes all the effects modeled in HPOP1, plus the atmospheric drag and the solar radiation pressure (SRP). Both Jacchia-Roberts and MSISE90 can be alternatively selected as atmospheric drag model, while for the solar activity the $F10.7$ and A_p indices are taken as per ECSS guidelines [33], under three levels of solar activity (low, moderate and high).

HPOP1 is adopted for all the analyses related to the nominal configuration of the constellation, being the atmospheric drag and SRP closely related to the mission operating epoch, which is currently still not defined. HPOP2 is considered for the CubeSat lifetime assessment and for the robustness analyses of the nominal configurations. The orbital propagators work with a time step

equal to 60 s. High fidelity propagators were validated by comparison with commercial tools. The ephemerides of the satellites are the input of the visibility tool, implemented in MATLAB environment, and developed for the estimation of the GRBs detected and triangulated by the constellation taking into account the scientific requirements. In all analyses, 1 Apr 2022 at 12:00 UTC was conventionally considered as the initial epoch (since, of course, the date of injection into orbit of the constellation is yet to be decided).

The tool, for each combination of three S/C (triplet) obtainable with the considered satellites, takes their trajectories as input and evaluates the triangulable GRBs during the mission lifetime (2 years), through the following procedure. For each time-span it is verified in the following order that: *a*) the three S/C are outside the forbidden regions; *b*) all the physical baselines are ≥ 1000 km; *c*) at least two projected baselines greater than the mean LoS are ≥ 1000 km. If the previous step is overtook, the triplet is considered as a potential co-observing group and the instantaneous FoVs overlapping is computed. At each time-span, the FoVs overlapping each triplet are added up to remove potential redundancies (if a sky portion is observed by several triplets, it is considered only one time). The tA parameter is computed, integrated over the lifetime and converted in detectable GRBs by means of the factor $\alpha_{GBM} = 0.083$ GRB/sr/day. Fig. 2 summarises the flow diagram of the logical operations processed by the mission analysis software tools.

3. Nominal orbits

This section illustrates the strategies adopted to identify the nominal orbits of the constellation satellites. The main goal is to maximise the number of triangulable GRBs with good localisation. The FoVs overlapping and the baseline distance requirement are in some cases in contrast. Thus, a compromise solution is required, with the aim to avoid over complication in mission operations, that could lead to practical infeasibility, avoiding at the same time an excessive, although inevitable, reduction in the scientific performance. The scientific

Figure 2: Flowchart of the mission analysis software tool.

requirement concerning the forbidden regions in Section 2.2 requires a preliminary parametric analysis over the orbit inclination to minimise the transits of satellites in the forbidden areas. Furthermore, due to the reasons explained in *Orbital requirements* (Section 2.2), orbits with a nominal altitude of 550 km have been considered. This value represents a good compromise between the need to preserve the payload and to limit the effects of atmospheric drag on orbital decay, therefore on the lifetime. Taking into account a group of co-observing satellites, defined as a group of N spacecraft sharing a non-null portion of overlapped FoV, it is evident that if the transits of each satellite in the forbidden regions do not occur simultaneously the operational time of the triplet reduces considerably. The interval for which the co-observing group is not able to produce measurement will be given by the amount of the residence time of any satellite in the forbidden areas. This suggests to consider nominal orbits so that, for the S/C of each co-observing group, a wide overlap in the transit in forbidden regions is verified. However the other mission requirements on the physical baseline (≥ 1000 km) and projected baseline (≥ 1000 km) are in conflict with the overlapping in the forbidden regions transits. The constraint on physical baseline, implies that two satellites cannot be too close. Moreover, in case of zenithal pointing, in order to have at least two projected baselines over 1000 km, different orbital planes for the satellites in a co-observing group must be considered. The guidelines considered to identify the nominal orbits are the following:

- Pairs of satellites for which the physical baseline is approximately 1500 km and is close to a frozen-condition are identified; it means that the physical baseline is quasi-constant during the satellites lifetime. These pairs will be called *leader pairs*. The main advantage of the leader pairs is that the S/C transit in forbidden regions in a quasi-simultaneous time. Furthermore the FoV overlap between the satellites in one leader pair is continuously high (about the 90 % of the FoVs is always overlapping).

- A third satellite, called *complementary satellite*, is related to each leader pair, completing a *nominal triplet*. This satellite, generally orbiting in a

distinct orbital plane, shall guarantee that the projected baseline between itself and the two leader satellites is large enough to satisfy the requirement ($\geq 1000\,\mathrm{km}$). At the same time it shall assure a good overlapping with the leader pair FoVs in order to have the maximum number of triangulable GRBs. While the leader pairs show a moderate interaction (in terms of overlap) with the other ones, each complementary satellite works with the other leader pairs generating also a non-nominal triplet, which allows a significant increase of the scientific performance of each constellation. This strategy allows a high level of modularity for the constellation, keeping the global performance sufficiently high even if the satellites are not all placed in orbit at the same time.

- The total orbital planes number shall be the minimum which allows to obtain a reasonable number of detected GRBs. The total orbital planes number shall be the minimum in order to minimise the launch campaign (therefore the total cost of the mission) and to reduce the time required for the orbital injection of the entire constellation. In this context, the strategy chosen in this work is minimise the overall number of orbital planes, at the expense of reducing the total number of triangulable GRBs.

The identification of the leader pairs and complementary satellites orbital elements was the result of an in-depth sensitivity analysis whose aim was to maximise the triangulated GRBs using the least number of orbital planes. A similar strategy could be adopted to have larger (quasi-frozen) projected baselines, for example of 3000 km. This would improve the accuracy of the localisation of transient events but, on the other hand, it would cause a considerable reduction in the overlap between the FoV of the triplet satellites, decreasing the number of detectable GRBs.

3.1. Forbidden regions analysis

Fig. 3 shows the forbidden regions mask (SAA and high radiation flux polar regions) plotted at 550 km, nominal altitude of the considered orbits.

A parametric analysis on inclination and LAN (Longitude of the Ascending Node) has been carried out. As LAN we refer to the geographical longitude, measured from the Greenwich meridian in the ECEF (Earth-centered, Earth-fixed) reference frame, where the satellite ground track intersects the inertial equator from south to north. Therefore, the LAN varies over time as a function of the reference meridian position. The aim is to identify the relationship between these orbital elements and the residence time of a S/C in the forbidden regions, in which the scientific instrument cannot operate. For this investigation the LPOP propagator was used, since the perturbative forces have reduced effects on the variation of the inclination. Analyses were conducted by varying the inclination between 0° and 90° and the LAN between 0° and 360° with a step equal to 1°. For retrograde inclinations, symmetry with respect to polar inclination $i = 90°$ can be taken into account. A propagation time of 2 years has been considered.

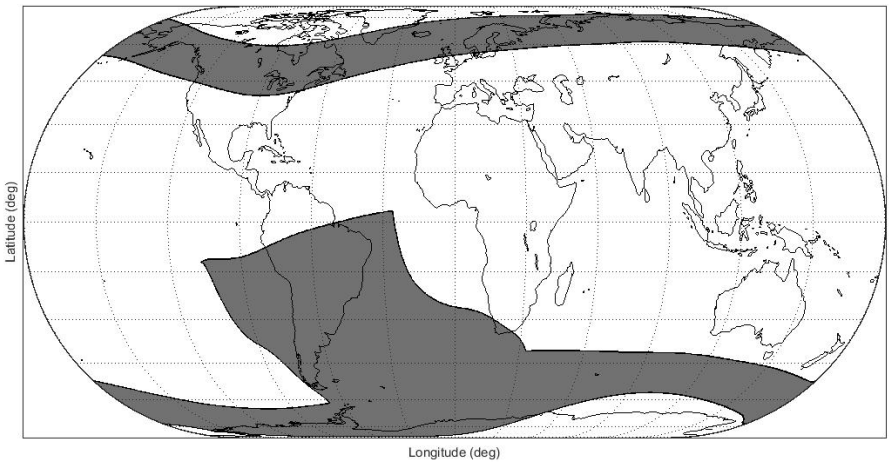

Figure 3: Forbidden regions mask (in grey). High flux areas in which the scientific instrument shall not be used: South Atlantic Anomaly (SAA) and high radiation flux polar regions at an altitude of 550 km.

Fig. 4 shows the percentage of the spacecraft lifetime spent inside the forbidden regions as function of the orbital plane inclination over the equator, with an error bar showing the influence of initial LAN. For inclinations up to 39° the total transit time in the forbidden regions is less remarkable than for medium and polar inclinations (the S/C avoids the polar regions). Therefore the optimal

inclinations are the quasi-equatorial ones and, in particular, the inclination for which the permanence time in SAA is minimum, is equal to 4° (about 6 %). For polar and quasi-polar inclinations the time for which the scientific instrument of each satellite cannot be used is over 30 % of their own lifetime. It is important to remark that inclinations between 30° and 70° cannot be considered due to scientific constraints. Considering only a zenithal pointing strategy to avoid attitude manoeuvres dedicated to scientific observations, to perform triangulations also on polar areas, satellites on non-equatorial orbital planes must also be considered. For these reasons, it will be necessary to distribute the satellites on both quasi-equatorial and quasi-polar inclinations.

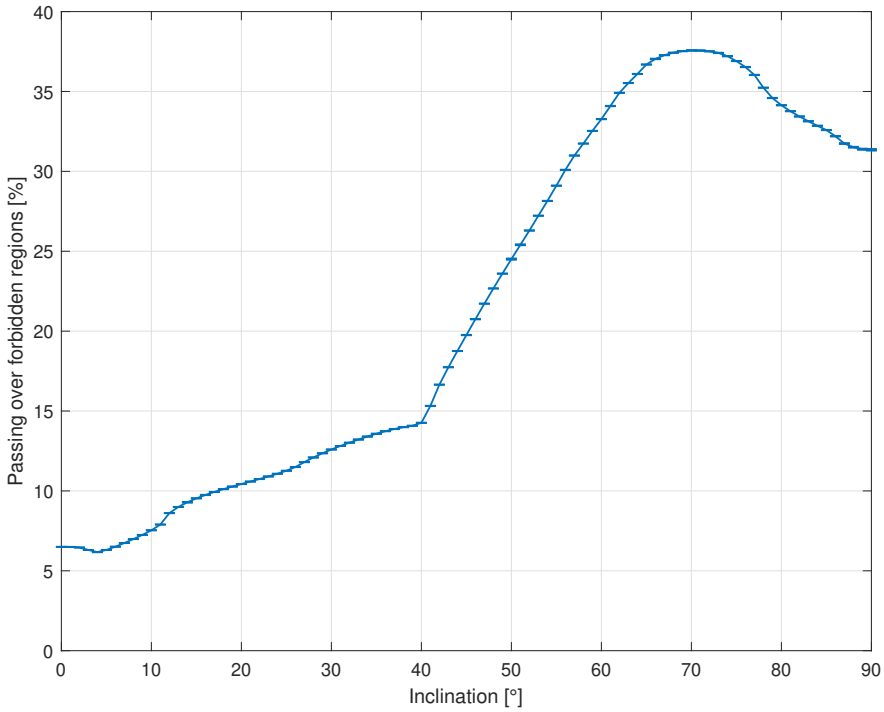

Figure 4: Percentage of residence time in forbidden regions (SAA and poles) as function of the orbital inclination.

3.2. Leader pairs

For the constellation design, an equatorial nucleus from 7 up to 9 satellites has been planned. This group has been extended up to 11, 12 or 14 S/C with the sun-synchronous satellites. This modulation allows the planning of the in-orbit insertion of the S/C in different epochs. Leader pairs have been investigated, for equatorial and polar inclinations, under the constraint to maintain the physical baseline between the satellites within the range [1000, 1500] km. This has required an analysis of differential orbital perturbations for the considered inclinations. For this analysis the propagation profile HPOP1 has been considered. The reference epoch was fixed at 1 Apr 2022 at 12:00 UTC; and for all nominal orbits a circular orbit ($e = 0$) with a semimajor axis $a = 6928.00\,\text{km}$ (at an altitude of 550 km with respect to the equatorial radius) and an Argument of Perigee $AoP = 0°$ have been fixed. The output of this analysis are the values of the LAN for which the physical baseline between pairs of satellites remains quasi-frozen. Three leader pairs have been defined for quasi-equatorial inclinations (A, B, C) which allow higher performance. Since, due to higher permanence in the forbidden regions, the SSO scientific performance reduces considerably, only two polar leader pairs (D and E) have been considered. Table 1 summarises the initial nominal values of the orbital elements at the presumed launch epoch; the subsequent behavior of the orbital elements is determined by the orbital perturbations. In this table the TA is the true anomaly, while the RAAN is the right ascension of the ascending node (i.e., the longitude of the ascending node measured in the J2000 inertial reference frame), which is correlated to the LAN, as a function of the epoch, by the Greenwich location in the J2000.

The table highlights how the leader pairs orbit on only three orbital planes: A and B are over an orbital plane with $i = 4.00°$ which minimise the transits in forbidden regions. The last equatorial leader pair (C) has been placed at $i = 7.8°$; this inclination allows a strong interaction (in the sense of capability to triangulate GRBs) between this pair and the other equatorial ones. For equatorial pairs, the physical baseline can be (approximately) frozen at about 1500 km for an initial true anomaly phase between the pair's satellites (Δf)

Table 1: Leader pairs ($h = 550\,\text{km}$, $a = 6928\,\text{km}$, $e = 1e-6$).

Satellite	i (deg)	RAAN (deg)	LAN (deg)	TA (deg)
SAT1A	4.00	80.20	70.65	0.00
SAT2A	4.00	80.20	70.65	14.00
SAT1B	4.00	80.20	70.65	130.00
SAT2B	4.00	80.20	70.65	144.00
SAT1C	7.80	156.50	146.95	5.00
SAT2C	7.80	156.50	146.95	351.00
SAT1D	97.72	99.55	90.00	354.80
SAT2D	97.72	99.55	90.00	5.00
SAT1E	97.72	99.55	90.00	175.00
SAT2E	97.72	99.55	90.00	185.00

close to 14°. Polar orbits shall be considered for detecting the GRBs in the high latitude regions. Although at these inclinations the permanence in forbidden regions is minimum for $i = 90°$, the sun-synchronous *dawn/dusk* orbit has been considered in reason of the multiple technical advantages that this solution can offer [34]. At the considered epoch, for $a = 6928\,\text{km}$ the nominal SSO dawn/dusk orbit can be obtained for $i = 97.72°$ and $LAN = 90.00°$ ($RAAN = 99.55°$). The sun-synchronous dawn/dusk LAN/RAAN is a function of the epoch. For SSO inclination the differential perturbations are more accentuated compared to equatorial orbits and the physical baseline can be frozen only for $\Delta f \approx 10°$ and for exact values of the initial true anomaly.

3.3. Complementary satellites

Complementary satellites provide at each leader pair a third satellite, which completes the nominal triplet, able to create at least two projected baselines $\geq 1000\,\text{km}$ in the co-observing group. In addition they maximise the number of detectable GRBs, not only for the nominal triplet, but also for the whole constellation configuration. For the quasi-equatorial planes, an optimal difference of 3.80° in the inclination (Δi) between the leader pair orbital plane and the one of the complementary satellite has been identified through a sensitivity analysis to identify the solution for which the maximum number of GRBs was triangulated. A constrain included in this investigation has been the reduction

of the overall orbital planes (this justifies the choice of $i = 7.80$ degree for the leader pair C). For this inclination delta, choosing appropriate values of the LAN and true anomaly of the complementary, it is possible to meet the projected baseline requirement and contextually contain the physical baselines between the complementary and the leader satellites within quasi-constant values. This allows a good overlapping among the FoVs of the entire triplet, and consequently to obtain a high rate of detectable GRBs. Fig. 5 and Fig. 6 well show this behaviour for the nominal triplet A. Fig. 5 illustrates the evolution of the projected baselines of the S/C of the triplet: while the projected baselines between the complementary satellite $SAT1C$ and the leaders constantly remain > 1000 km (green and royal blue lines), the one between $SAT1A$ and $SAT1B$ is always < 1000 km (lime-colored line); these three baselines remain, simultaneously, less than 3000 km. On the other hand Fig. 6 shows how the physical baselines among the three satellites are without interruption > 1000 km. As noted, projected-baselines greater than thousands of kilometres would allow to obtain higher scientific performances in terms of accuracy in the positioning of the transient event. This suggests the possibility of adding satellites to the constellation, placed on appropriately chosen orbits, with the aim of increasing the projected-baselines between the satellites of a co-observing group. This strategy would increase the scientific return, at the price of a decrease in the technological performance of the constellation, in terms of triangulated GRB/spacecraft.

A dedicated investigation for dawn/dusk SSO leader pairs has highlighted that there is no Δi for which quasi-frozen physical and projected baselines can be obtained. For this reason, orbit at SSO inclination with different LAN shall be considered. Only one complementary satellite (SSO_CS) which presents an optimal interaction (in terms of triangulable GRBs) with both the SSO leader pairs has been considered. Indeed, the reduced marginality allowed by other complementary SSO satellites, suggests considering only one of these for both the SSO leader pairs. Table 2 recapitulates the complementary satellites initial orbital elements at the presumed launch epoch. Including them, the maximum number of satellites here considered for the constellation configurations reaches

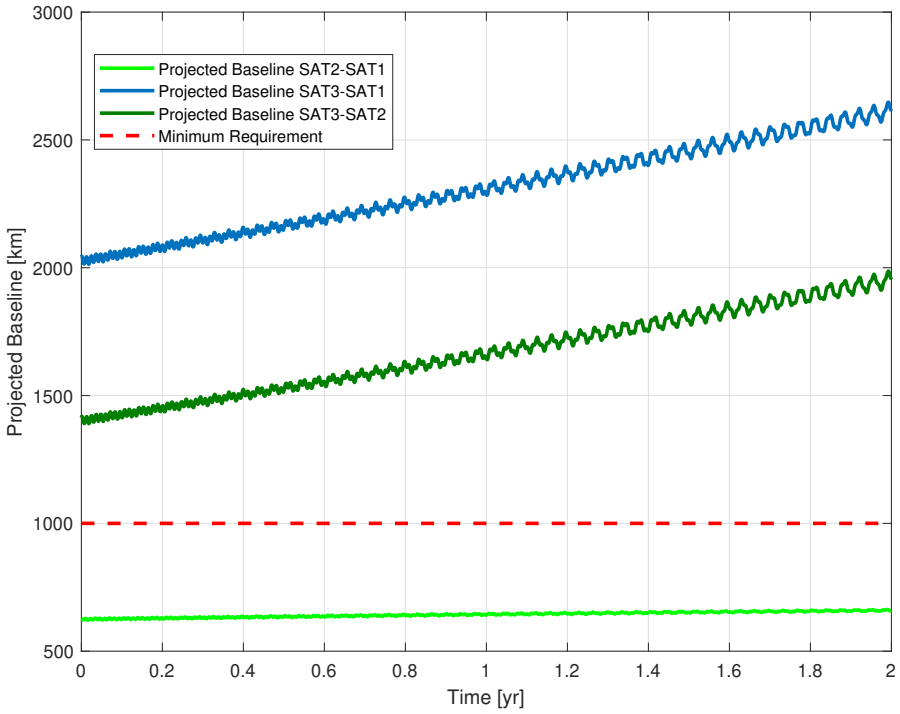

Figure 5: Projected baselines evolution for the nominal triplet A. It is required that the projected baseline shall be ≥ 1000 km for at least two pairs of elements in a group of N_{co-obs} satellites.

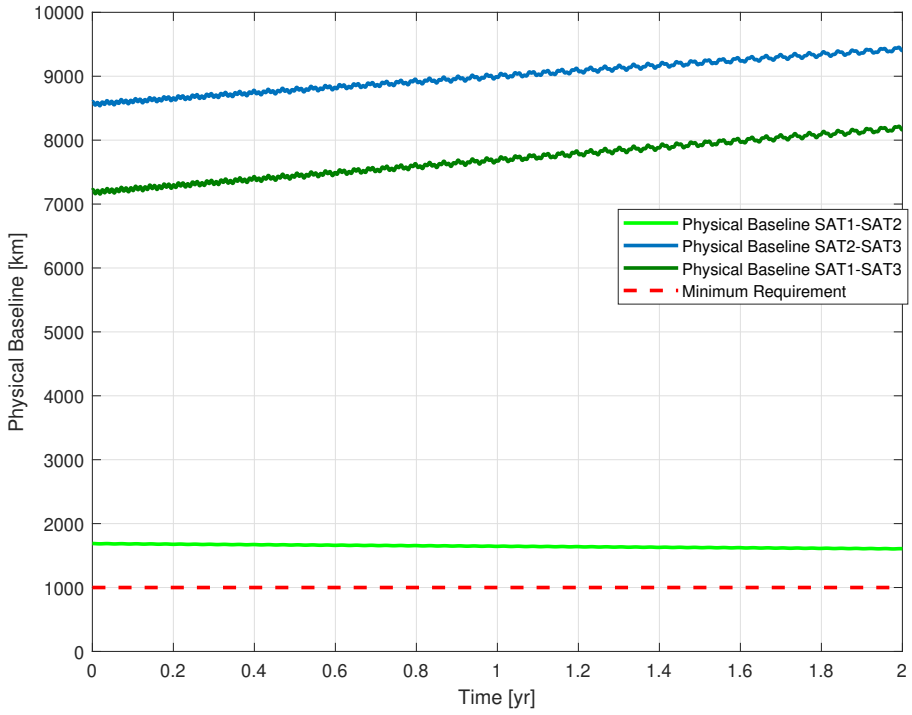

Figure 6: Physical baselines evolution for the nominal triplet A.

Table 2: Complementary satellites ($h = 550\,\text{km}$, $a = 6928\,\text{km}$, $e = 1e-6$).

Satellite	i (deg)	RAAN (deg)	LAN (deg)	TA (deg)
SAT3A	7.80	19.00	9.45	0.00
SAT3B	7.80	19.00	9.45	342.00
SAT3C	4.00	80.20	70.65	24.00
SSO_CS	97.72	336.00	326.45	0

the value of 14. The next section presents the modulation opportunities related to the constellation configurations up to 14 S/C and shows how the addition of further SSO spacecraft decrease the mean detectable GRBs per satellite.

4. Constellation configurations

This section is dedicated to the presentation of the constellation extension by a minimum of 7 up to 14 spacecraft. As explained in Section 2.3 a dedicated MATLAB tool has been built to evaluate the number of triangulable GRBs for each configuration. Equatorial satellites generally allow the detection of a higher number of GRBs compared to the SSOs (as seen, mainly due to shorter transit times in forbidden regions). For this reason, the former ones shall be primarily considered, compared to the latter, in the orbit insertion. The nominal configurations were built to have a strong interaction between leader pairs and complementary satellites of different nominal triplets which allows a mean triangulable GRBs in line with the goal ($\eta \geq 20$). In other words the performance of each configuration is higher than the one obtainable by summing the performance of the nominal triplets that compose the constellation. For example, the triplet A triangulates 45 GRBs during its lifetime whenever considered alone ($\eta \sim 15$); once inserted in the complete constellation the leader pair of the same triplet works also with complementary satellites nominally belonging to other triplets, achieving $\eta > 20$. Two typologies of nominal configuration have been planned mixing leader pairs described in Table 1 with correspondent complementary satellites of Table 2:

a) *Equatorial-only configurations*, up to 9 satellites:

- FC-7, with nominal triplet A plus the leader pairs B and C;
- FC-8, with nominal triplets A and C plus the leader pair B;
- FC-9, with the three equatorial nominal triplets A, B and C, i.e., composed of all the satellites of Table 1;

b) *Equatorial and SSO configurations*, up to 14 satellites:

- FC-11, with the three triplets of the FC-9 plus the SSO leader pair D;
- FC-12, with the satellites of the FC-11 plus the complementary satellite SSO_CS;
- FC-14, with the satellites of the FC-12 plus the SSO leader pair E, i.e., composed of all the satellites of Table 1 and Table 2.

The first ground-track at the reference epoch (1 Apr 2022 at 12:00 UTC) of each satellite for each configuration is shown in Figures 7-12. In these figures, each color identifies a nominal triplet, whilst the yellow portion of the figures indicates the sunlighted area.

Table 3 reports the performance of the nominal configurations. The % and Sr/Day columns indicate the observed sky portion, in percentage and solid angle terms. The GRBs column reports the total number of triangulable GRBs during the two-years mission lifetime for each configuration. The last column reports the η efficiency parameter which, as mentioned, is computed as the total number of GRBs triangulated by the constellation divided by the number of the nanosatellites that compose it. Its maximum value is obtained by FC-9 ($\eta = 22.15$) composed by all the equatorial S/C. When further equatorial satellites are added the increment in the overall performance is marginal, suggesting that the FC-9 configuration is enough to practically completely cover the sky in the equatorial band. The only way to significantly increase the total number of detected GRBs is the addition of sun-synchronous satellites to the constellation, at the price of a decrease in the constellation performance. Indeed, for FC-14, η drops below the threshold, fixed as a goal, of 20. For this reason, a further

Table 3: Nominal constellation configurations.

Configuration	%	Sr/Day	GRBs	η
FC-7	18.80	2.36	143.13	20.45
FC-8	22.74	2.86	173.18	21.65
FC-9	26.18	3.29	199.39	22.15
FC-11	29.76	3.74	226.74	20.61
FC-12	31.68	3.98	241.34	20.11
FC-14	35.62	4.47	271.41	19.39

extension of the constellation is not taken into account. In the next subsection, more considerations about this aspect are reported.

4.1. Further satellites

In this paper, constellation configurations with at most 9 equatorial S/C and 5 SSO S/C have been considered. The parameter used to discriminate the efficiency of the constellation was only the ratio between the number of triangulable Gamma Ray Bursts (simultaneously detected by at least three nanosatellites) detected by the constellation and the total number of nanosatellites over the two-years lifetime (i.e., η). The overall size of the constellation could obviously be extended with other equatorial or polar satellites but, in this case, the η parameter degrades. In example a constellation of 11 S/C, composed by the FC-9 satellites plus an another optimal equatorial leader pair (in the same orbital plane of the A and B pairs, with the same characteristics in terms of quasi-frozen physical baseline), would guarantee only 17 GRBs more than the nominal FC-9. This occurs because the 9 equatorial S/C are arranged in order to contain the redundancies between the nominal leader pairs. Therefore the additional leader pairs allow, mainly, to "re-detect" GRBs already observed by the nominal FC-9 satellites. As regards further SSO satellites, every additional sun-synchronous S/C can increase the total number of detected GRBs, but produces a deterioration in the overall efficiency in terms of η parameter. This is the product of two combined effects: primarily the permanence of the SSO satellites in the forbidden regions (more than 30 % of the lifetime); in second order, the redundancy in the equatorial belt (with the first 9 satellites). Adding more satellites in quasi-polar orbits would

cause the decrease of η under the fixed goal.

Thus, when only the zenithal-pointing is considered, and the attitude manoeuvres are not performed, the contemporary injection in orbit of a large number of satellites on the one hand allows the constellation a reduced marginality in the performance of any additional S/C. In other words, each additional satellite allows a number of GRBs certainly lower than 20 to be triangulated. Under this point of view, if a large number of satellites (e.g., > 25) shall be considered for the full constellation, the results obtained in the present analysis suggest that spreading the satellites over a longer period of time with respect to the nominal mission duration of two years (considering, for example, a periodic replacement of the satellites) allows the detection of a higher total number of GRBs during the entire mission. On the other hand, the injection of many satellites into orbit at the same time could be fruitful for several reasons. First, it will allow us to have spare satellites, properly positioned for each configuration, to remedy the potential early-failure of one or more CubeSat. Secondly, since by adding more units the same GRB is detected by a higher number of satellites, the scientific performance of the mission improves; indeed, the positioning accuracy increases by a factor of $\sqrt{N_{co-obs} - 3}$ according to Eq.(1). Moreover, since positioning improves as the projected baseline between satellites increases, additional CubeSats can be exploited to maintain projected baselines between co-observing satellites greater than several thousand kilometres. Observing the same GRB with many satellites also increases the effective area, then collecting more photons. Furthermore, the detection of one event by several sensors allows to optimise the detection by selecting the sensors able to measure photons with low incidence angles. Finally many contemporaneous satellites would allow an all-sky monitor, which is the main purpose of the HERMES Full Constellation.

5. Robustness analysis

In this section, the robustness of the constellation performance has been analysed. Particularly the effects of atmospheric drag and SRP perturbations

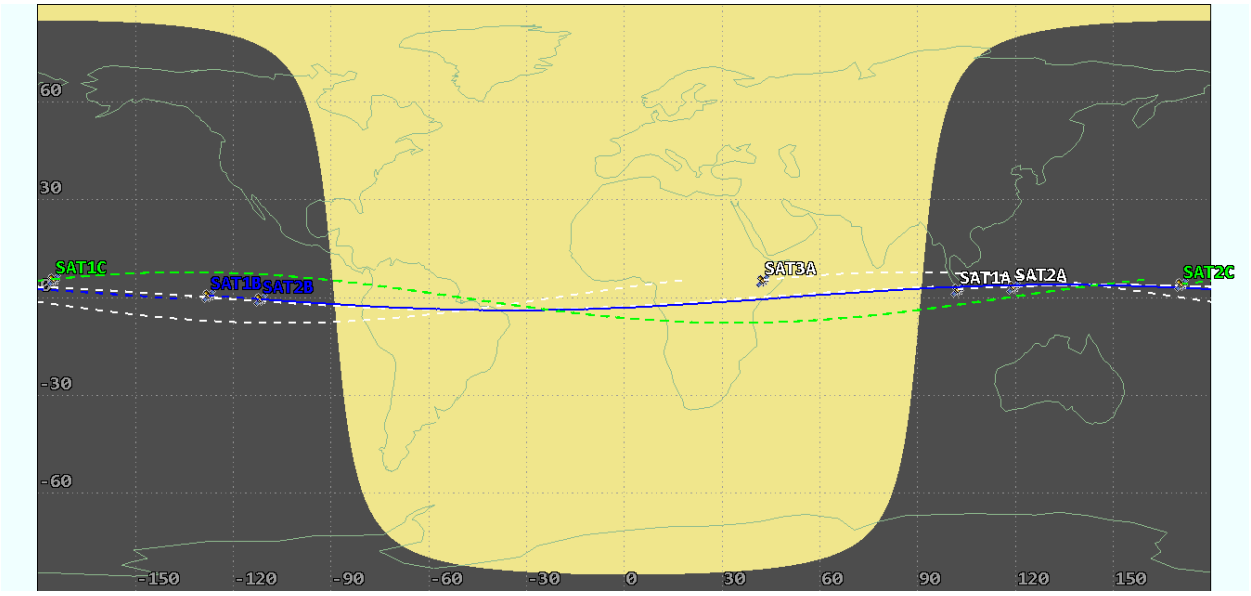

Figure 7: First ground-tracks of the FC-7 configuration at the reference epoch. White ground tracks refer to the triplet A, blue and green tracks refer to leader pairs B and C (images elaborated with AGI - Systems Tool Kit 12.0 software).

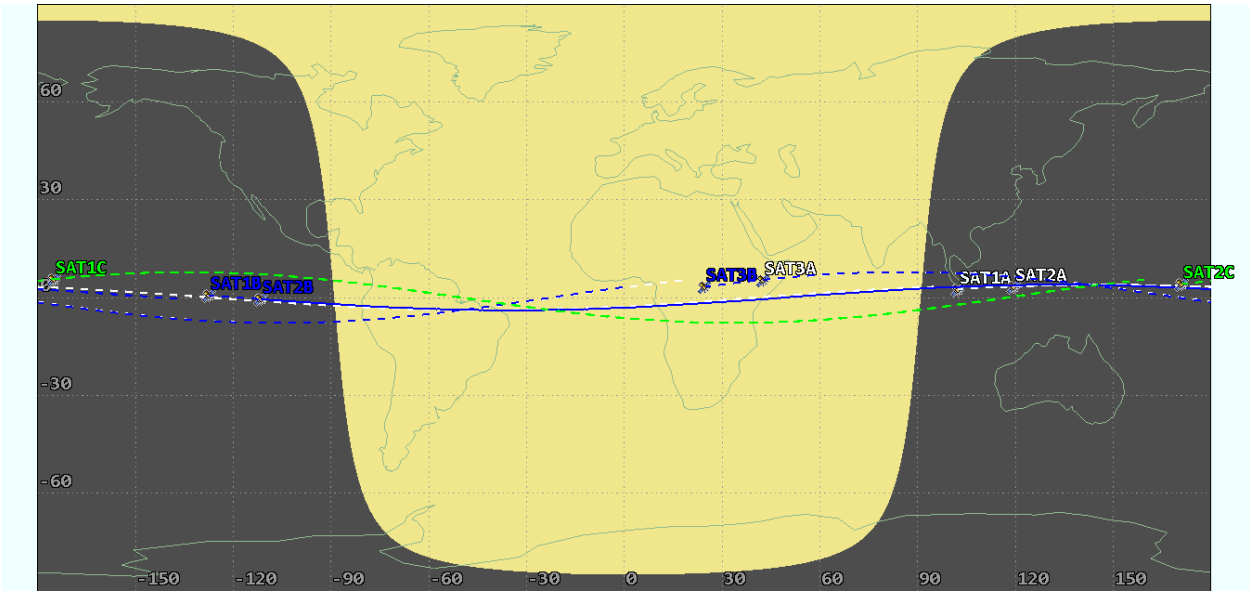

Figure 8: First ground-tracks of the FC-8 configuration at the reference epoch. White and blue ground tracks refer to the triplet A and B, green tracks refer to leader pair C (images elaborated with AGI - Systems Tool Kit 12.0 software).

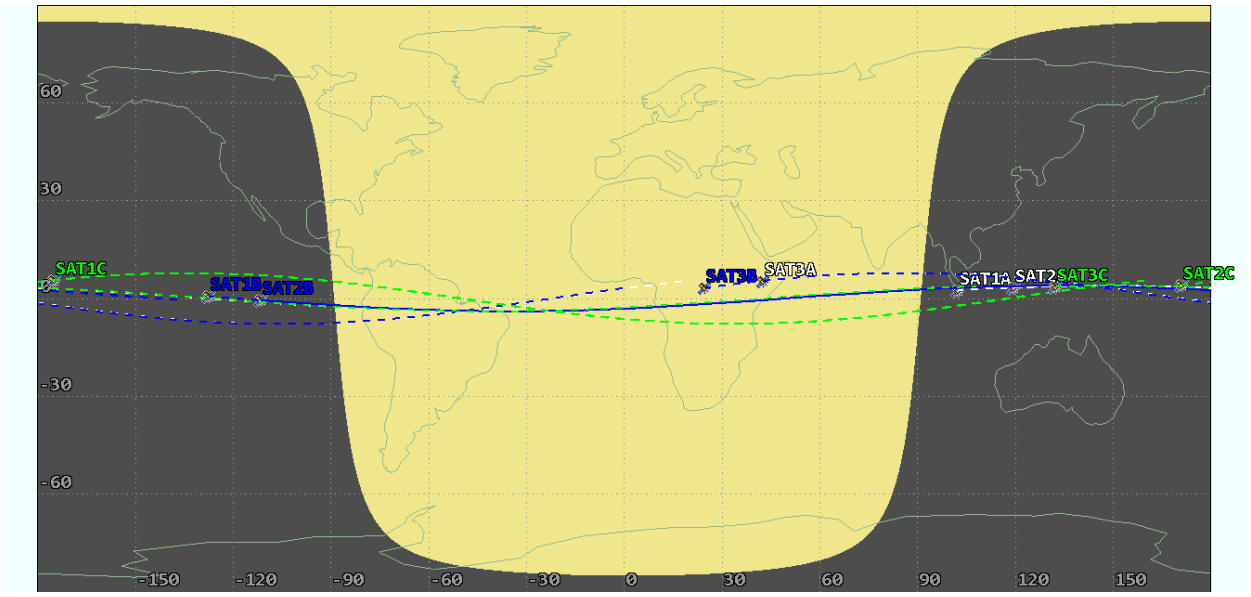

Figure 9: First ground-tracks of the FC-9 configuration at the reference epoch. This configuration consists of all equatorial satellites: white, blue and green tracks refer to triplets A, B and C (images elaborated with AGI - Systems Tool Kit 12.0 software).

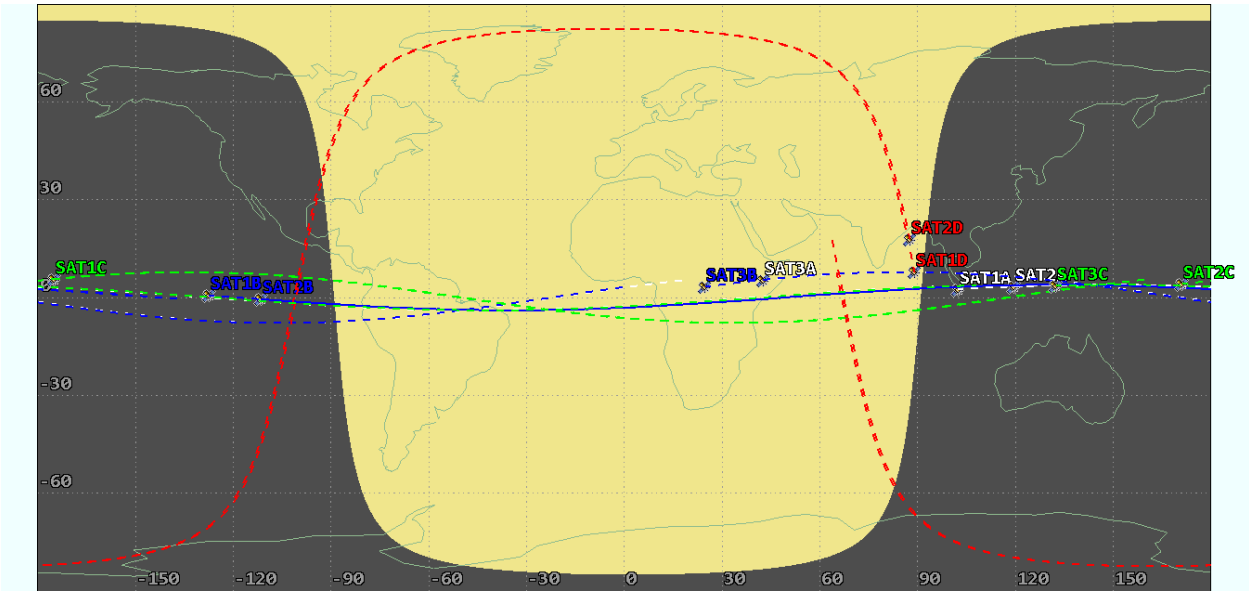

Figure 10: First ground-tracks of the FC-11 configuration at the reference epoch. This configuration consists of all equatorial satellites (white, blue and green tracks refer to triplets A, B and C) plus SSO leader pair D in red (images elaborated with AGI - Systems Tool Kit 12.0 software).

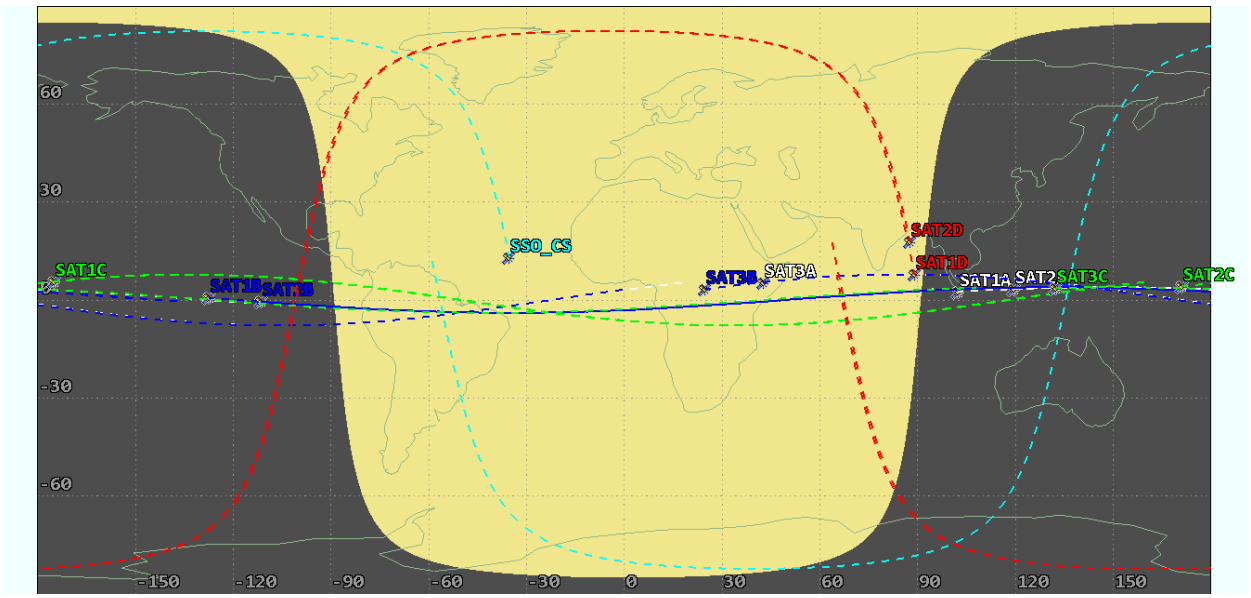

Figure 11: First ground-tracks of the FC-12 configuration at the reference epoch. This configuration consists of all equatorial satellites (white, blue and green tracks refer to triplets A, B and C) plus SSO leader pair D (red tracks) and the SSO_CS unit in cyan (images elaborated with AGI - Systems Tool Kit 12.0 software).

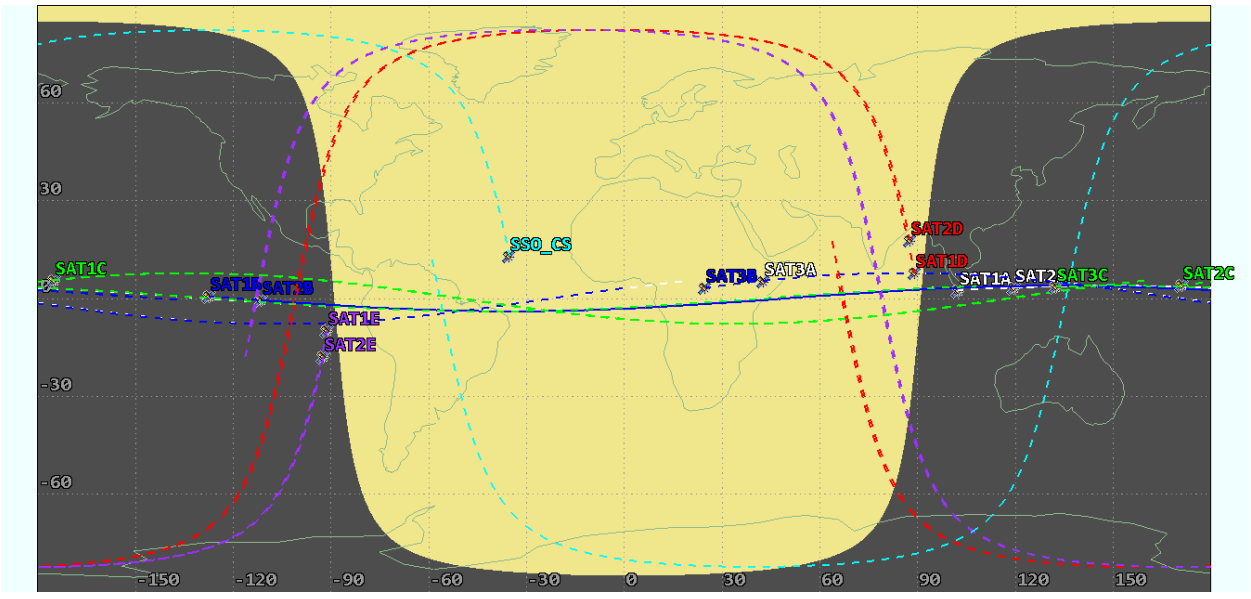

Figure 12: First ground-tracks of the FC-14 configuration at the reference epoch. This configuration consists of all equatorial and SSO satellites: white, blue and green tracks refer to equatorial triplets A, B and C; red and violet trackes refer to SSO leader pairs D and E; cyan track refers to SSO_CS unit (images elaborated with AGI - Systems Tool Kit 12.0 software).

Table 4: Solar index values.

Long-Term			
Index	Low	Moderate	High
F10.7	65	140	250
Ap	0	15	45
Short-Term			
Index	Low	Moderate	High
F10.7	65	140	300
Ap	0	15	240

as well as the failure of one S/C will be considered. The consequences of these effects over the number of detectable GRBs will be examined.

5.1. Atmospheric drag and SRP perturbative effects

HPOP1 orbital propagator does not consider the perturbative effects of atmospheric drag and SRP since they are not exactly predictable as they strongly depend on the solar activity (and on the launch epoch during the eleven-years-long solar cycle). For this reason these perturbative effects have been examined separately, throug HPOP2 orbital propagator, considering the three solar activity profiles recommended by the ECSS (low, moderate and high solar activity). Table 4 summarises the solar activity index values taken by ECSS standard [33]. In this analysis, a realistic value for HERMES CubeSat of mass to area ratio in the order of $50\,\mathrm{kg/m^2}$ has been considered. Since, given the nature of the mission, based on small satellites, and as already mentioned, no station-keeping manoeuvres are planned, a first check is that the semi-major axis remains high enough to ensure a lifetime which fulfils the requirements. For high solar activity, the minimum semi-major axis after 2 years reaches the value of about 6880 km (corresponding to $h \approx 500\,\mathrm{km}$). Table 5 reports the performance for the nominal constellation configurations taking into account the above-mentioned solar activity profiles. The worst conditions have been observed for high solar activity; in that case the complete constellation could triangulate a minimum mean value of about 18.15 GRBs per S/C. For FC-8 and FC-9 configurations the goal $\eta \geq 20$ is always achieved.

Table 5: Performance considering atmospheric drag and SRP.

Solar Activity:	Low		Moderate		High	
Configuration	GRBs	η	GRBs	η	GRBs	η
FC-7	141.85	20.26	140.36	20.05	130.94	18.71
FC-8	172.40	21.55	171.52	21.44	162.40	20.30
FC-9	198.38	22.04	196.24	21.80	186.83	20.75
FC-11	225.85	20.53	223.85	20.35	214.88	19.53
FC-12	240.54	20.05	238.46	19.87	230.16	19.18
FC-14	269.79	19.27	265.33	18.95	254.15	18.15

5.2. Early-Failures analysis

A second analysed aspect is the early-failure of one satellite, in order to identify the minimum number of detectable GRBs when one spacecraft is not able to cooperate with the others. This aspect is very relevant considering that the design of the constellations is based on the leader pairs concept. The objective of this robustness analysis is to answer to the question: when one of the units of a nominal constellation is unable to work, does the constellation's performance remain consistent with the mission requirements? The analysis has been conducted by simulating the failure of each unit of each constellation, and then computing the number of detected GRBs by the remaining satellites. For example, for the FC-9 the failure of each of the 9 nanosatellites has been simulated and then the triangulated GRBs by the remaining 8 units were computed. For each configuration the worst case corresponds to the failure of the unit for which the number of detected GRBs reaches its minimum. The analysis has been carried out with HPOP1 propagator (no drag and no SRP) since the real operating scenario, especially in terms of atmospheric density, will be closely connected to the launch epoch and, in particular, to its position with respect to the eleven-years-long solar activity cycle. Therefore, it has been preferred to analyse the effects of drag (and SRP) separately.

Table 6 reports the results of the investigation. The η efficiency parameter is calculated taking into account only the active satellites. The early-failure of one satellite is an event particularly critical for FC-7, indeed in this case η could be less than 15. However the table shows that the early-failure of one satellite is

Table 6: Early-failures analysis results.

Equatorial-only				
Configuration	Min		Max	
	GRBs	η	GRBs	η
FC-7	83.61	13.94	115.91	19.32
FC-8	114.56	16.37	143.21	20.46
FC-9	152.47	19.06	173.29	21.66
Equatorial + Polar				
Configuration	Min		Max	
	GRBs	η	GRBs	η
FC-11	182.70	18.27	200.71	20.07
FC-12	199.07	18.10	228.38	20.76
FC-14	232.04	17.85	258.52	19.89

an event that can be accepted without a marked (or unacceptable) loss in the performance: η remains close to the goal of 20. Moreover an early-failure causes decreasing effects with the increasing of the total number of the S/C.

6. Conclusion

A mission analysis, which intends to be propaedeutic for the HERMES Full Constellation design, consisting of at least seven CubeSats, has been presented. In the case of a large constellation the performance for each nanosatellite has been estimated for several configurations, based on orbital planes with quasi-equatorial and quasi-polar inclinations, without station-keeping and optimal pointing manoeuvres. An average number of 20 triangulable Gamma Ray Bursts (simultaneously detected by at least three nanosatellites) detected by each nanosatellite over the two years life-time (i.e., η) has been used to discriminate the performance of the constellations. In particular, the number of detectable and triangulable GRBs by each configuration, as a function of the number of satellites forming the constellation, have been estimated.

The quasi-equatorial orbital inclinations are preferable as they limit the transits of satellite platforms in forbidden areas (SAA and polar regions). Nevertheless using only satellites on quasi-equatorial orbital planes, the performances (in terms of η) of constellations composed by more than 9 quasi-equatorial satellites

rapidly decrease, due to the redundancies between the different nanosatellites. By adding S/C on sun-synchronous orbits, the performance remains in line with requirements only for constellations including up to fourteen nanosatellites; for larger ones, η drops below the threshold of 20. In this way, as the size of the constellation increases, overall performance deteriorates in terms of η.

The perturbative effects of atmospheric drag and solar radiation pressure do not have a significant impact over the number of detectable GRBs. Furthermore, the early-failure of a CubeSat produces generally non-irreparable effects.

In conclusion, if it is desired to linearly increase the raw total number of triangulated GRBs by increasing the number of satellites in the constellation, it appears more convenient to distribute them along a longer time span, with respect to have all of them contemporary in orbit for just 2 years (spare satellites can be in any case considered to limit the failures of other CubeSats). On the other hand, it must be considered that the accuracy in localising the transient event is directly proportional to the number of CubeSats that detect the GRB and to the average baseline between them. Therefore, the simultaneous injection into orbit of tens, or even hundreds, of nanosatellites, against a number of GRBs detected by each payload lower than the initial goal, allows to increase the accuracy of the triangulation up to few arcmin. Furthermore, a higher number of satellites would allow to increase the effective area and then improving the data quality by collecting more counts in the detectors from the astrophysical sources.

At this point, a further development is to identify the minimum number of satellites such as to obtain an all-sky monitor in which, simultaneously, every point of the sky is observed by at least three detectors. In this way, any transient event could be detected and triangulated. With the current HFC mission constraints this is not an easy goal to achieve, especially for mid-latitudes sky coverage. By removing the constraint on inclinations, the complete coverage of mid-latitudes by the constellation would be possible even without pointing manoeuvres. An all-sky monitor constellation thus obtained would inevitably produce redundancies, with most of the GRBs detected by more than 3 units.

On the one hand, this significantly deteriorates the η parameter but, on the other hand, it allows a more accurate localisation of the transient event and, increasing the collecting area, the improving of the data quality by collecting more counts in the detectors from the astrophysical sources. This issues will be investigated in a future work.

Acknowledgments

The authors acknowledge the team at PoliMi involved in the project and, in particular, the rest of the mission analysis group: Dr Andrea Colagrossi, Jacopo Prinetto and Stefano Silvestrini. Furthermore, we acknowledge Dr Fabrizio Fiore from INAF Osservatorio Astronomico di Trieste (Principal Investigator for HERMES project) and Dr Andrea Sanna from Università di Cagliari for the useful suggestions that have allowed us to improve the paper. We also thank the Italian Space Agency (ASI) and the scientific partners of HERMES-TP, the Istituto Nazionale di Astrofisica, Università degli Studi di Cagliari, Università degli Studi di Palermo.
The analysis have been performed with the aid of the IT resources made available by the computer centre of the "Dipartimento di Matematica" at the University of Roma Tor Vergata and, in particular, with the HPE ProLiant DL 380 server ("Ipazia") (`http://www.mat.uniroma2.it/Calcolo/hardware/ipazia_accesso.php`) part of MIUR Excellence Project 2018-2022 "MATH@TOV" (CUP E83C18000100006).

Funding

For this work M.C. was supported by INdAM (Istituto Nazionale di Alta Matematica) via F46C18000040005 grant “HERMES Technological Pathfinder – HTP”.

References

[1] R. W. Klebesadel, I. B. Strong, R. A. Olson, Observations of gamma-ray bursts of cosmic origin, The Astrophysical Journal 182 (1973) L85. https://ui.adsabs.harvard.edu/link_gateway/1973ApJ...182L..85K/doi:10.1086/181225.

[2] B. P. Abbott, R. Abbott, T. Abbott, F. Acernese, K. Ackley, C. Adams, T. Adams, P. Addesso, R. Adhikari, V. Adya, et al., Gravitational waves and gamma-rays from a binary neutron star merger: Gw170817 and grb 170817a, The Astrophysical Journal Letters 848 (2) (2017) L13. https://dx.doi.org/10.3847/2041--8213/aa920c.

[3] B. P. Abbott, R. Abbott, T. Abbott, F. Acernese, K. Ackley, C. Adams, T. Adams, P. Addesso, R. Adhikari, V. Adya, et al., Gw170817: observation of gravitational waves from a binary neutron star inspiral, Physical Review Letters 119 (16) (2017) 161101. https://dx.doi.org/10.1103/PhysRevLett.119.161101.

[4] G. Boella, R. Butler, G. Perola, L. Piro, L. Scarsi, J. Bleeker, Bepposax, the wide band mission for x-ray astronomy, Astronomy and Astrophysics Supplement Series 122 (2) (1997) 299–307. https://dx.doi.org/10.1051/aas:1997136.

[5] C. Winkler, G. Di Cocco, N. Gehrels, A. Giménez, S. Grebenev, W. Hermsen, J. Mas-Hesse, F. Lebrun, N. Lund, G. Palumbo, et al., The integral mission, Astronomy & Astrophysics 411 (1) (2003) L1–L6. https://dx.doi.org/10.1051/0004--6361:20031288.

[6] N. Gehrels, G. Chincarini, P. Giommi, K. Mason, J. A. Nousek, A. Wells, N. White, S. Barthelmy, D. N. Burrows, L. Cominsky, et al., The swift gamma-ray burst mission, The Astrophysical Journal 611 (2) (2004) 1005. https://dx.doi.org/10.1063/1.1810924.

[7] M. Feroci, E. Costa, P. Soffitta, E. Del Monte, G. Di Persio, I. Donnarumma, Y. Evangelista, M. Frutti, I. Lapshov, F. Lazzarotto, et al., Superagile: The hard x-ray imager for the agile space mission, Nuclear Instruments and Methods in Physics Research Section A: Accelerators, Spectrometers, Detectors and Associated Equipment 581 (3) (2007) 728–754. https://dx.doi.org/10.1016/j.nima.2007.07.147.

[8] M. Tavani, G. Barbiellini, A. Argan, F. Boffelli, A. Bulgarelli, P. Caraveo, P. Cattaneo, A. Chen, V. Cocco, E. Costa, et al., The agile mission, Astronomy & Astrophysics 502 (3) (2009) 995–1013. https://dx.doi.org/10.1051/0004--6361/200810527.

[9] C. Meegan, G. Lichti, P. Bhat, E. Bissaldi, M. S. Briggs, V. Connaughton, R. Diehl, G. Fishman, J. Greiner, A. S. Hoover, et al., The fermi gamma-ray burst monitor, The Astrophysical Journal 702 (1) (2009) 791.

[10] W. Atwood, A. A. Abdo, M. Ackermann, W. Althouse, B. Anderson, M. Axelsson, L. Baldini, J. Ballet, D. Band, G. Barbiellini, et al., The large area telescope on the fermi gamma-ray space telescope mission, The Astrophysical Journal 697 (2) (2009) 1071.

[11] N. Gehrels, D. Spergel, et al., Wide-field infrared survey telescope (wfirst) mission and synergies with lisa and ligo-virgo, in: Journal of physics: conference series, Vol. 610, IOP Publishing, 2015, pp. 012007. https://dx.doi.org/10.1088/1742--6596/610/1/012007.

[12] X. Barcons, K. Nandra, D. Barret, J. Den Herder, A. Fabian, L. Piro, M. G. Watson, et al., Athena: the x-ray observatory to study the hot and energetic universe, in: Journal of Physics: Conference Series, Vol. 610, IOP Publishing, 2015, pp. 012008. http://dx.doi.org/10.1088/1742--6596/610/1/012008.

[13] F. Pajot, D. Barret, T. Lam-Trong, J.-W. Den Herder, L. Piro, M. Cappi, J. Huovelin, R. Kelley, J. Mas-Hesse, K. Mitsuda, et al., The athena x-ray

integral field unit (x-ifu), Journal of Low Temperature Physics 193 (5-6) (2018) 901–907. https://dx.doi.org/10.1007/s10909--018--1904--5.

[14] F. Fiore, L. Burderi, M. Lavagna, R. Bertacin, Y. Evangelista, R. Campana, F. Fuschino, P. Lunghi, A. Monge, B. Negri, et al., The hermes-technologic and scientific pathfinder, in: Space Telescopes and Instrumentation 2020: Ultraviolet to Gamma Ray, Vol. 11444, International Society for Optics and Photonics, 2020, p. 114441R. https://doi.org/10.1117/12.2560680.

[15] F. Fiore, L. Burderi, T. Di Salvo, M. Feroci, C. Labanti, M. R. Lavagna, S. Pirrotta, Hermes: a swarm of nano-satellites for high energy astrophysics and fundamental physics, in: Space Telescopes and Instrumentation 2018: Ultraviolet to Gamma Ray, Vol. 10699, International Society for Optics and Photonics, 2018, p. 106992Q. https://dx.doi.org/10.1117/12.2311980.

[16] L. Burderi, F. Fiore, A. Papitto, A. Sanna, T. Di Salvo, A. Riggio, The hermes project (high energy rapid modular ensemble of satellites): Probing space-time quantum foam and hunting for gravitational wave electromagnetic counterpart, cosp 42 (2018) E1–17. https://doi.org/10.1117/12.2561779.

[17] M. Grassi, M. Gandola, F. Mele, G. Bertuccio, P. Malcovati, F. Fuschino, R. Campana, C. Labanti, M. Fiorini, Y. Evangelista, et al., X-/γ-ray detection instrument for the hermes nano-satellites based on sdds read-out by the lyra mixed-signal asic chipset, in: 2020 IEEE International Instrumentation and Measurement Technology Conference (I2MTC), IEEE, 2020, pp. 1–6. https://doi.org/10.1109/I2MTC43012.2020.9129520.

[18] H. Heidt, J. Puig-Suari, A. Moore, S. Nakasuka, R. Twiggs, Cubesat: A new generation of picosatellite for education and industry low-cost space experimentation (2000).

[19] J. Puig-Suari, C. Turner, W. Ahlgren, Development of the standard cubesat deployer and a cubesat class picosatellite, in: 2001 IEEE aerospace conference proceedings (cat. No. 01TH8542), Vol. 1, IEEE, 2001, pp. 1–347. https://dx.doi.org/10.1109/AERO.2001.931726.

[20] A. Poghosyan, A. Golkar, Cubesat evolution: Analyzing cubesat capabilities for conducting science missions, Progress in Aerospace Sciences 88 (2017) 59–83. https://doi.org/10.1016/j.paerosci.2016.11.002.

[21] L. Burderi, T. Di Salvo, A. Riggio, A. F. Gambino, Grailquest and hermes: hunting for gravitational wave electromagnetic counterparts and probing space-time quantum foam, in: Space Telescopes and Instrumentation 2020: Ultraviolet to Gamma Ray, Vol. 11444, International Society for Optics and Photonics, 2020, p. 114444Y. https://doi.org/10.1117/12.2561779.

[22] F. Fuschino, R. Campana, C. Labanti, Y. Evangelista, M. Feroci, L. Burderi, F. Fiore, F. Ambrosino, G. Baldazzi, P. Bellutti, et al., Hermes: An ultra-wide band x and gamma-ray transient monitor on board a nano-satellite constellation, Nuclear Instruments and Methods in Physics Research Section A: Accelerators, Spectrometers, Detectors and Associated Equipment 936 (2019) 199–203. https://dx.doi.org/10.1016/j.nima.2018.11.072.

[23] Y. Evangelista, F. Fiore, F. Fuschino, R. Campana, F. Ceraudo, E. Demenev, A. Guzman, C. Labanti, G. La Rosa, M. Fiorini, et al., The scientific payload on-board the hermes-tp and hermes-sp cubesat missions, in: Space Telescopes and Instrumentation 2020: Ultraviolet to Gamma Ray, Vol. 11444, International Society for Optics and Photonics, 2020, p. 114441T. https://doi.org/10.1117/12.2561018.

[24] A. Colagrossi, J. Prinetto, S. Silvestrini, M. Orfano, M. Lavagna, F. Fiore, L. Burderi, R. Bertacin, S. Pirrotta, Semi-analytical approach to fasten complex and flexible pointing strategies definition for nanosatellite clusters: the hermes mission case from design to flight, in: 70th International Astronautical Congress (IAC 2019), 2019, pp. 1–8.

[25] A. Colagrossi, S. Silvestrini, J. Prinetto, M. Lavagna, Hermes: a cubesat based constellation for the new generation of multi-messenger astrophysics, in: 2020 AAS/AIAA Astrodynamics Specialist Conference, 2020, pp. 1–20.

[26] F. Scala, G. Zanotti, S. Curzel, M. Fetescu, P. Lunghi, M. Lavagna, R. Bertacin, The hermes mission: A cubesat constellation for multi-messenger astrophysics, in: 5th IAA Conference on University Satellite Missions and CubeSat Workshop, 2020, pp. 1–17.

[27] A. Colagrossi, J. Prinetto, S. Silvestrini, M. R. Lavagna, Sky visibility analysis for astrophysical data return maximization in hermes constellation, Journal of Astronomical Telescopes, Instruments, and Systems 6 (4) (2020) 048001. https://doi.org/10.1117/1.JATIS.6.4.048001.

[28] J. Řípa, G. Dilillo, R. Campana, G. Galgóczi, A comparison of trapped particle models in low earth orbit, in: Space Telescopes and Instrumentation 2020: Ultraviolet to Gamma Ray, Vol. 11444, International Society for Optics and Photonics, 2020, p. 114443P. https://doi.org/10.1117/12.2561011.

[29] D. Gruber, A. Goldstein, V. W. von Ahlefeld, P. N. Bhat, E. Bissaldi, M. S. Briggs, D. Byrne, W. H. Cleveland, V. Connaughton, R. Diehl, et al., The fermi gbm gamma-ray burst spectral catalog: four years of data, The Astrophysical Journal Supplement Series 211 (1) (2014) 12. https://dx.doi.org/10.1088/0067--0049/211/1/12.

[30] G. Ghirlanda, R. Salvaterra, G. Ghisellini, S. Mereghetti, G. Tagliaferri, S. Campana, J. P. Osborne, P. O'Brien, N. Tanvir, D. Willingale, et al., Accessing the population of high-redshift gamma ray bursts, Monthly Notices of the Royal Astronomical Society 448 (3) (2015) 2514–2524.

[31] N. K. Pavlis, S. A. Holmes, S. C. Kenyon, J. K. Factor, The development and evaluation of the earth gravitational model 2008 (egm2008), Journal of geophysical research: solid earth 117 (B4) (2012) 1–38. https://dx.doi.org/10.1029/2011JB008916.

[32] W. M. Folkner, J. G. Williams, D. H. Boggs, R. S. Park, P. Kuchynka, The planetary and lunar ephemerides de430 and de431, Interplanetary Network Progress Report 196 (1) (2014) 1–15. https://doi.org/10.3847/1538--3881/abd414.

[33] E. Secretariat, Ecss space engineering-space environment, Tech. rep., Technical Report ECSS-E-ST-10-04C, ESA (2008).

[34] A. Anselmi, G. Catastini, Design of the gg satellite, Physics Letters A 318 (3) (2003) 205–212. https://dx.doi.org/10.1016/j.physleta.2003.07.023.